Equation of state for methane in nanoporous material at supercritical temperature over a wide range of pressure

Conference Paper · January 2016

DOI: 10.2118/180085-MS

CITATIONS
0

READS
31

2 authors, including:

Keliu Wu
The University of Calgary
52 PUBLICATIONS **132** CITATIONS

SEE PROFILE

SPE-180085-MS

Equation of state for methane in nanoporous material at supercritical temperature over a wide range of pressure

Keliu Wu, University of Calgary; Zhangxin John Chen, University of Calgary

This paper was prepared for presentation at the SPE Europec featured at 78th EAGE Conference and Exhibition held in Vienna, Austria, 30 May – 2 June 2016.

Abstract

The methane storage behavior in nanoporous material is significantly different from bulk phase, and has a fundamental role in methane extraction from shale and its storage for vehicular applications. Here we show that the behavior and mechanisms of the methane storage are mainly dominated by the ratio of the interaction between methane molecules and nanopores wall to the methane intermolecular interaction, and the geometric constraint. By linking the macroscopic properties of methane storage to the microscopic properties of methane molecules-nanopores wall molecules system, we develop an equation of state for methane at supercritical temperature over a wide range of pressure. Molecular dynamic simulation data demonstrate that this equation is able to relate very well the methane storage behavior with each of key physical parameters, including pore size, shape, wall chemistry and roughness. Moreover, this equation only requires one fitted parameter, and is simply and powerful in application.

Introduction

Rapidly rising population from today 7 billion, to about 9 billion estimated by 2050, and about 10 billion estimated by 2100[1], will place tremendous energy demand around the world[2], increasing from about 12 billion tonne oil equivalents (t.o.e.) in 2009 to either 17 billion t.o.e. or 18 billion t.o.e. by 2035 predicated by the International Energy Agency based in Paris[3]. With the unavoidable depletion of conventional petroleum-based fuels and the serious greenhouse effect[4, 5], natural gas, consisting mainly of methane, is an attractive and potential ″bridge fuel″ during transition to a carbon-free fuels[6] due to its abundant reserves[7–10], wide distribution[11], low CO_2 emission[12] and economic efficiency[4].

During the past decade, horizontal drilling and hydraulic fracturing make successful extraction of natural gas from shale economically feasible[13]. Shale, characterized by abundant nanopores, including organic kerogen pores and inorganic pores, hosts free gas and adsorbed gas because of large internal surface area[14]. In addition, these nanopores are irregular in cross section, including bubble-like, elliptical and faveolated shapes[15]. Therefore, these nanopores cause a huge challenge in shale gas extraction, such as gas reserve estimation, numerical simulation, and production predication. Increasing improvements in shale gas extraction has driven a renewed interested in natural gas application in transportation[16]. However, the main technological barrier for the widespread use of natural gas as an alternative vehicular fuel is the relatively low volumetric energy density compared with gasoline[17, 18]. Adsorbed natural gas

may more potentially overcome this barrier comparing with conventional storage technologies, including compressed natural gas and liquefied natural gas [4,5,7,16,17]. Adsorbed natural gas technology may store more natural gas at much lower pressure with lower cost and better safety[18, 19]. To accelerate the vehicular application of nature gas, the US Department of Energy has set an ambitious target of a volumetric storage capacity of 350 cm^3 (STP) cm^{-3} (adsorbent) and a gravimetric storage capacity of 0.5 g (CH_4) g^{-1} (adsorbent) at operational conditions[20, 21]. It is a formidable challenge for chemists and material scientists to exploit a novel technology to achieve this goa[17, 18]. Significant researches have been conducted about adsorbed natural gas in nanoporous materials: zeolites[22-24], zeolitic imidazolate frameworks[25-29], nanoporous carbons[30-31], porous organic polymer networks[32], covalent organic frameworks[33], and metal-organic frameworks (MOFs) [34-37]. MOFs, a relatively new family of nanoporous materials, have become very important in gases storage applications because that they can be designed from the atomic scale, and tailored systematically in chemical composition, functionality, and pore size to maximize natural gas storage capacity[10,38]. From those elaborated above, it is concluded that the storage of methane molecules in nanoporous materials is a fundamental and long-standing challengeable issue for shale gas reserve estimation, extraction, and its application in transportation.

To better understand and manipulate the methane storage in nanoporous materials, it is key to shed light on its underlying mechanisms. Methane storage behavior in nanoporous materials arises primarily from the interaction between methane molecules and nanopores wall[30], and is also influenced by the intermolecular interaction of methane, especially for the case at high pressure[39]. Nanopore size[5,40], shape[12,38], wall chemistry[5,7,18], wall roughness[41], and operational conditions including pressure[16] and temperature[42], inducing the varying ratio of two interaction strengths mentioned above, influence the methane storage behavior in a single nanopore. Similarly, the methane storage behavior for nanoporous materials is also controlled by porosity[43-44], nanopore size distribution[45], nanopore connectivity[24], and specific surface area[31, 44, 46]. Methane mainly is stored in micropores (<2 nm) or mesopores (2 nm~50 nm) at supercritical temperature (above 273.15 K) over a wide range of pressure (up to 50 MPa) during the process for shale gas extraction and its application in transportation. Under such extreme surrounding conditions, the methane storage behavior is significantly complex, and has not been studied to our knowledge. However, understanding and manipulating methane storage behavior is crucial to extract successfully methane from shale formation[11] and move it to market in vehicular applications[5, 43, 47].

Gas storage behavior in nanoporous materials can be investigated through experiments[5, 14, 48-50], molecular dynamic (MD) simulations[8,11,46,51], mathematical models[47,52-53], and combining these methods[54-55]. Experiments are the closest to reality, furthermore, with rapid advancement in experimental equipment and technology today, it is possible by direct observation to open out some undiscovered and underlying mechanisms, such as adsorption sites determination[49], adsorbed gas molecules structures and ordering[50]. However, experiments are expensive, time-consuming[47], and hard to identify the effect of single key parameter[30]. MD simulations and mathematical models, inevitable complements to experiments, may predict and verify experimental results, even reveal the undiscovered experimental phenomenon[56, 57]. Although recent advances have greatly enhanced computational performance, due to the large number of atoms and force field calculations involved in modeling gas storage behavior, MD simulations are still be computationally expensive and time-consuming, with each case requiring a separate modeling, compared with mathematical models[30]. In contrast, a practical mathematical model, based on some assumptions and approximations, not only provides instantaneous calculation results, identifies each effect of some key physical parameters, but also makes general predictions and observations[47, 52-53]. These advantages of mathematical models are especially remarkable in modeling gas storage behavior in nanoporous materials. For example, methane storage behavior in complex nanoporous shale is varying during the depressurized development process of shale gas reservoirs, while conducting numerical simulation using a mathematical model for production prediction, millions of computational grids need to participate in this calculation. In another typical example, MOFs, a most potential microporous materials

in vehicular applications, are synthesized from modular molecular building blocks, typically metal clusters and organic linkers[45]. They can, in principle, be assembled to construct an almost unlimited number of MOFs[17]. Over the past few years, thousands of novel MOFs have been synthesized in indoor experiments[58]. Thus, it is a huge task to screen extensively and rapidly nanoporous materials to identify the best candidates for methane storage in vehicular application.

In this communication, we have developed a computationally efficient equation of state (EOS) for methane in nanoporous materials at supercritical temperature over a wide range of pressure. Our equation takes into account the interaction between methane molecules and nanopore walls, methane intermolecular interaction, and the varying ratio of both interactions with pressure. In particular, our equation is able to describe the methane storage in nanoporous shale at pressures up to 50 MPa where its storage behavior is significantly different from the counterpart at low pressure, such as methane storage in vehicular application. Furthermore, application of our equation requires only an unknown constant that can be determined by fitting experimental data or MD simulations results. Due to the simple and robust nature of our equation, it is readily extended to other gases. We use our equation to investigate the methane storage behavior in nanoporous materials at supercritical temperature over a wide range of pressure, elucidate each effect of nanoporous material properties (e.g., nanopore size, shape, wall chemistry, wall roughness, etc.), and enhance our understanding of the correlation between gas storage behavior and nanoporous material properties. Our work provides an effective and powerful tool for modeling shale gas storage behavior, and screening and designing of nanoporous materials for methane storage in vehicular application.

Behavior and mechanisms of gas storage in nanoporous material

The gas storage behavior in nanoporous materials is controlled by its mechanisms. Some of the gas storage mechanisms can be revealed by the advanced experimental technologies today, for example, the gas storage properties (adsorbed gas density and layers number) characterized by the Nuclear Magnetic Resonance[14], even the adsorption sites and the ordering of adsorbed gas molecules detected by in situ small-angle X-ray scattering[49, 50]. The gas storage mechanisms are mainly dominated by the ratio of the interaction between gas molecules and nanopores wall to gas intermolecular interaction[8, 39, 59]. For gas storage in nanopores with walls of homogeneous chemical and physical properties, while the interaction between gas molecules and nanopores wall dominates ($F_{S\text{-}F}/F_{F\text{-}F} > 1$), gas storage amount first increases sharply with pressure in the low pressure region, then slowly in the relatively high pressure region[11, 60], and finally becomes a constant due to the storage saturation limited by the space available for the gas molecules[61] (see Fig. 1a). Similar but different in the low pressure region[5], gas storage behaviors for $F_{S\text{-}F}/F_{F\text{-}F} = 1$ and $F_{S\text{-}F}/F_{F\text{-}F} < 1$, are shown in Fig. 1b and c, respectively. The both interactions mentioned above primarily arise from the van der Waal forces, including Keesom force (two permanent dipoles), Debye force (a permanent dipole and a corresponding induced dipole), and London dispersion force (two instantaneously induced dipoles) [62]. For gas storage in nanopores with walls of heterogeneous chemical and physical properties, in the low pressure region, gas molecules first prefer to adsorb at strong adsorption sites induced by Keesom force (see **I** region in Fig. 1d and e) or at small groves due to the roughness on wall (not shown in Fig. 1d and e), then adsorb at the relatively weak adsorption sites induced by Debye force (see **II** region in Fig. 1d and e). While the pressure increases to the middle pressure region, weak London dispersion force exerted by the adsorbed gas molecules dominates the gas storage behavior[49, 51] because the strong and relatively weak adsorption sites have been largely occupied by the adsorbed gas molecules (see **III** region in Fig. 1d and e). While the pressure continues to increase to the relatively high pressure region, the gas storage behavior in nanopores is somewhat similar to that in bulk gas phase due to the dominance of free gas intermolecular interactions (see **IV** region in Fig. 1d and e). Finally, gas storage amount becomes almost unvarying in the high pressure region due to the storage saturation, furthermore, is lower than that in bulk gas phase (see **V** region in Fig. 1d and e).

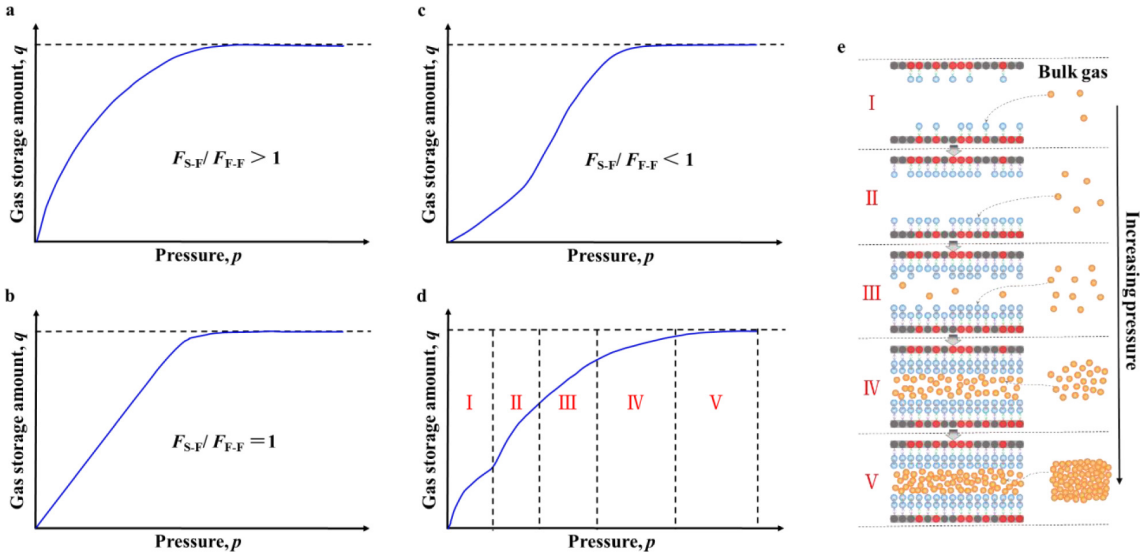

Figure 1—Schematic representation of gas storage at supercritical temperature in nanopores with different interactions. For gas storage behavior in nanopores with walls of homogeneous chemical and physical properties: (a) Strong fluid-wall interaction; (b) Middle fluid-wall interaction; (c) Weak fluid-wall interaction. For gas storage in nanopores with walls of heterogeneous chemical and physical properties, (d) gas storage behavior, and (e) gas storage mechanisms, red, wall molecules with the strong adsorption sites; light black, wall molecules with the relatively weak adsorption sites; light blue, adsorbed gas molecules; orange, free gas molecules; green arrows, strongly attractive interaction between gas molecules and the strong adsorption sites; purple arrows, weakly attractive interaction between gas molecules and the weak adsorption sites; yellow arrows, the adsorbed gas intermolecular interaction.

For nanoporous materials for methane storage in vehicular application, their working capacity (also called usable capacity or deliverable capacity), generally defined as the difference in methane storage amount between 0.5 MPa and 6.5 MPa, is more key than the total storage capacity[5]. To maximize the working capacity, we may optimize the number and distribution of the strong and weak adsorption sites on wall to achieve the relatively low methane storage amount in low pressure region (<0.5 MPa) and very high methane storage amount in relatively high pressure region (up to 6.5 MPa)[7,18, 63]. This is because that with increasing pressure, the attractive interaction between gas molecules and the weak adsorption sites gradually becomes to play more important role (see **II** region in Fig. 1d and e). For the methane storage at extremely high pressure (up to 50 MPa) in nanopores of shale gas reservoirs, compared with bulk gas phase, its storage amount is smaller (see **V** region in Fig. 1d and e) due to the limited available space in nanopores, furthermore, the interval between the first adsorption layer and the wall, about 3.575 Å consisted with the Lennard-Jones (LJ) parameter[11] (see Fig. 1e), also decreases the available space. In addition, the interaction between methane molecules and the wall also decreases methane storage amount due to the dominance of the methane intermolecular interaction at high pressure. However, it can enhance methane storage amount due to its dominance at relatively low pressure, more explanation is shown in discussion below. Thus, a powerful EOS for methane must capture these unique phenomenon in nanopores.

Capturing confinement effects

Gas thermodynamic properties in nanopores are significantly different from the corresponding bulk gas properties, which have been investigated well by the experiments, theory, and MD simulations[64-74]. These unique and interesting phenomenon are induced, on the one hand, by the geometric constraint limiting the gas molecules number[52], and on the other hand, by the non-negligible van der Waals forces arising from the interaction between gas molecules and wall in nanoporous materials[75]. Bulk gas molecules move randomly without specific orientation and direction, while the gas molecules confined in nanopores have a relatively well-ordered and layered structure in the axial direction (see Fig. 1e) induced by the geometric

constraint and the van der Waals forces exerted by nanopores wall. These structural differences cause the change in gas thermodynamic properties, especially for the critical properties including the critical temperature and critical pressure. The critical temperature and critical pressure both decrease as nanopores size decreases, even though the absence of the van der Waals forces[52]. In addition, the van der Waals forces influence and complicate the varying behaviors of the critical properties. The critical properties are dependent on several parameters, such as nanopores size, geometry, wall physical and chemical properties, and gas properties[76-77] because of these factors influencing the geometric constraint or the van der Waals forces mentioned above. The varying extents of the critical properties, as key parameters in modeling gas storage in nanoporous materials, can be determined by MD simulations, and fitted as known value in calculations of the EOS developed by us bellow (see Fig. 2). Generally, for gas confined in nanopores with the same nanopores geometry, the change of the critical properties are more noticeable for the stronger van der Waals forces and the smaller pores size; for gas confined in nanopores with the same nanopores size and van der Waals forces, the change is more noticeable in cylindrical nanopores compared with that in slit nanopores (see Fig. 2).

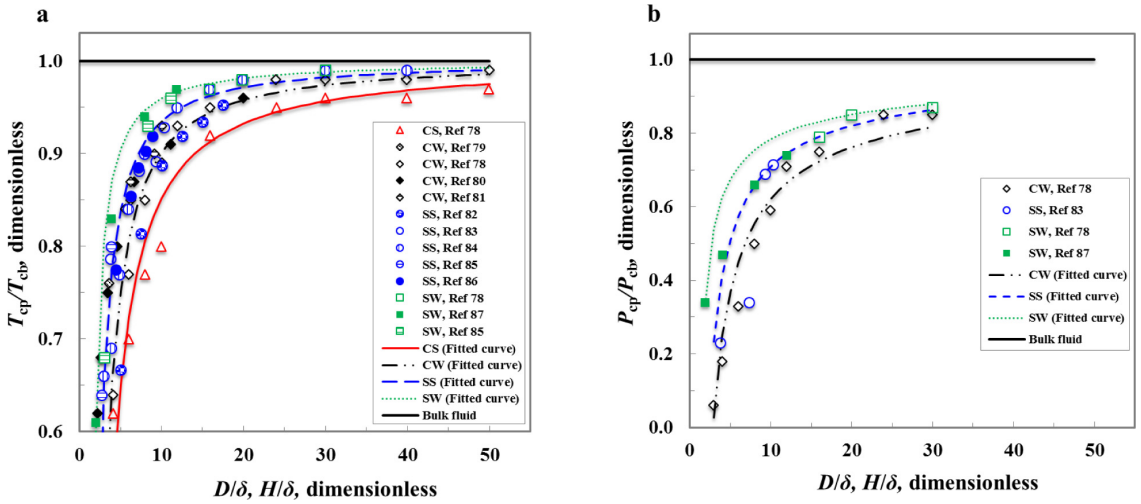

Figure 2—The dependence of critical properties (all reduced by the corresponding bulk values) on nanopore size. (a) Variation of critical temperature with nanopore size; (b) Variation of critical pressure with nanopore size. *D*, cylindrical nanopores diameter; *H*, slit nanopores width; δ, gas molecular diameter; T_{cp} is the critical temperature of gas in nanopores; T_{cb} is the critical temperature of bulk gas; P_{cp} is the critical pressure of gas in nanopores; P_{cb} is the critical pressure of bulk gas; CS, cylindrical nanopores with the strong adsorption sites; CW, cylindrical nanopores with the weak adsorption sites; SS, slit nanopores with the strong adsorption sites; SW, slit nanopores with the weak adsorption sites. Thick horizontal solid lines represent the bulk values. Curves along with symbols are fitted values.

Characterizing microscopic descriptors of different interactions

To depict exactly the gas storage behavior in nanoporous materials, the macroscopic properties of gas storage must link to the microscopic properties of gas molecules-wall molecules system[61]. The key descriptors of gas storage in nanoporous materials include the strength of the gas intermolecular interaction and the strength of the gas molecules-wall molecules interaction.

In low pressure regions (corresponding **I** and **II** regions in Fig. 1d and e), gas storage behavior is mainly controlled by the strength of the gas molecules-wall molecules interaction, which can be characterized by the Henry law equilibrium constant[88],

$$K_{\mathrm{h}} = \int_{v} e^{-\phi_{\mathrm{fs}}(x)/k_{\mathrm{B}}T}\,\mathrm{d}r \tag{1}$$

where, $\phi_{fs}(r)$ is the potential of gas molecules and wall; x is the coordinate; k_B is the Boltzmann constant; T is the temperature.

For a cylindrical pore, the well-known hypergeometric potential of gas molecules and wall is[89],

$$\phi_{fs}(r)=4\varepsilon_{fs}\rho_s\left(\delta_{fs}^{12}I_1-\delta_{fs}^{6}I_2\right) \tag{2}$$

where, ε_{fs} and δ_{fs} are the gas molecules–wall well depth and collision diameter of LJ parameters, respectively; ρ_s is the wall atomic density; r is the radial coordinate.

For a slit pore, the potential of gas molecules and wall following the Steele potential is[90, 91],

$$\phi_{fs}(h)=2\pi\varepsilon_{fs}\rho_s\delta_{fs}^2\left\{\left[\frac{2}{5}\left(\frac{\delta_{fs}}{h}\right)^{10}-\left(\frac{\delta_{fs}}{h}\right)^{4}\right]+\left[\frac{2}{5}\left(\frac{\delta_{fs}}{H-h}\right)^{10}-\left(\frac{\delta_{fs}}{H-h}\right)^{4}\right]\right\} \tag{3}$$

where, h is the distance away from a wall.

As shown in Eqs (2) and (3), a gas molecule interacts with the nearest atom of the wall, and the interaction strength is characterized by ε_{fs}. In addition, the gas molecule also interacts with all atoms of the wall within a certain cutoff distance, these multiple interactions are characterized by the surface atomic density ρ_s. For the case of wall roughness, the interaction is further augmented and characterized by the increasing ε_{fs} in our work. Thus, the gas storage behavior in low pressure region mainly depends on three physical parameters: gas molecules–wall well depth, wall atomic density, and wall roughness.

While the pressure increases (above the middle pressure region corresponding **III** and **IV** regions in Fig. 1d and e), the gas intermolecular interaction gradually becomes strong, non-negligible in contribution of gas storage behavior, and is determined by the intrinsic microscopic properties of the gas molecule, such as its shape, polarizability, and permanent electric moments[61]. The interaction strength can be characterized by the equilibrium constant for gas,

$$K_{ff}=\exp\left(-\phi_{ff}/k_BT\right) \tag{4}$$

where, ϕ_{ff} is the potential of gas molecules-molecules, and expressed as[61],

$$\phi_{ff}=\left(\frac{p_r}{p_{r\,max}}-1\right)^{p_r}\exp\left(\frac{p_r^2\varepsilon_{ff}}{k_BT}\right) \tag{5}$$

where, ε_{ff} is the gas molecules–molecules well depth of LJ parameters; p_r is the reduced pressure; p_{rmax} is the maximum reduced pressure.

Developing EOS for methane in nanoporous material

A practical and powerful EOS, for methane in nanoporous materials, must not only reduce the fitted parameters, but also capture the key methane storage mechanisms in different pressure regions. In the present work, we develop an EOS with only one fitted parameter, and our EOS links the methane storage behavior and the microscopic properties including the varying critical properties, the strength of the gas intermolecular interaction, and the strength of the gas molecules-wall molecules interaction as elucidated above.

In relatively high pressure region (**IV** region in Fig. 1d and e), the gas intermolecular interaction dominates the gas storage behavior, and this process can be quantitatively depicted by an appropriate EOS[61]. For methane at supercritical temperature, Redlich-Kwong (RK) EOS[92] is chosen as the basic equation for developing our EOS, due to its excellent prediction for light hydrocarbons in the supercritical region[93].

$$p = \frac{RT}{v-b} - \frac{a}{v(v+b)} \tag{6}$$

where, p is the pressure; R is the universal gas constant; v is the gas molar volume; $a=0.42748R^2T_c^{2}T_r^{-0.5}/p_c$, is ″attraction″ parameter; $b=0.08664\,RT_c/p_c$, is ″repulsion″ parameter; p_c is the critical pressure; T_c is the critical temperature; T_r is the reduced temperature.

In relatively low pressure regions (**I**, **II** and **III** regions in Fig. 1d and e), the interaction between gas molecules and wall is non-negligible, even dominates the gas storage behavior in **I** and **II** regions. The interaction depends on the nanopore size, shape, wall chemistry, atomic density, and roughness. The gas storage behavior is mainly controlled by the ratio of the interaction between gas molecules and wall to gas intermolecular interaction, which can be characterized by using the microscopic descriptors of the both interactions derived above (Eqs (1) and (4)),

$$K_{fs} = K_h^{\exp[A(1-K_{ff})]} \tag{7}$$

where, A is a positive and fitted parameter for a certain gas-nanoporous material system, and obtained by fitting the experimental results or MD data.

As shown in Eq (7), the ratio K_{fs} is a function of pressure and temperature. At a certain temperature, while the pressure increases to very high region, K_{fs} gradually becomes small and finally approaches to ″1″, indicating that the contribution of the interaction between gas molecules and wall gradually becomes small and finally negligible, while the contribution of gas intermolecular interaction gradually becomes large and finally dominates, which is similar to bulk gas; in contrast, while the pressure decreases to very low region, K_{fs} gradually becomes large and finally approaches to ″K_h″, indicating that the contribution of the interaction between gas molecules and wall gradually dominates, and may be quantified by the Henry law equilibrium constant at very low pressure. At a certain pressure, while the temperature is below a certain value, the gas molecules don't have enough kinetic energy to overcome the strength of van der Waals forces exerted by the wall[88], thus K_{fs} is large, and the contribution of the interaction between gas molecules and wall dominates; in contrast, while the temperature increases above a certain value, the gas molecules will have sufficient kinetic energy to escape from the wall attraction field in the vicinity of the wall[88], thus K_{fs} is small, and the contribution of the interaction between gas molecules and wall gradually becomes small and finally negligible.

In extremely high pressure region (region **V** in Fig. 1d and e), the gas storage is at the saturation due to the geometric constraint[61] and the van der Waals forces arising from the interaction between wall and gas molecules, and can be characterized by the varying critical properties of methane in nanoporous materials as mentioned above.

To cover these different methane storage mechanisms in different pressure regions, RK EOS need to be modified as follows

$$a' = aK_{fs} \tag{8}$$

$$b' = b/K_{fs} \tag{9}$$

In addition, it is noted that the critical temperature T_c and critical pressure p_c are both functions of pore size, shape, wall chemistry, atomic density and roughness as elucidated above, thus the confinement effects are also considered in this modified equation (our EOS).

Comparing our EOS with RK EOS, we see that our EOS makes two important improvements. First, the prediction of pseudo liquid behavior (at supercritical temperature) is more accurate because that b', the volume approaching a limiting value at extremely high pressure, accounts for the effects of different

interactions and the geometric constraint. Second, the prediction of nonideal behavior is improved due to *a*' also considering the effects of different interactions and the geometric constraint.

To validate our EOS for methane in nanoporous materials, we adopt the experimental results and MD data available in the published literature to compare with those calculated by our EOS. First, the choosing basic equation (RK EOS) is reliable in modeling the storage for bulk gas at supercritical temperature because of the excellent agreement with data collected by the National Institute of Standards and Technology (NIST)[94] (see Fig. 3a). Second, MD simulation data is accurate, and can be used to validate our EOS, because that MD simulation data[95] matches very well with those calculated by RK EOS (see Fig. 3b). Third, the results obtained by our EOS are consistent with MD simulation data for gas storage in nanoporous materials (see Fig. 3c). Despite the variety of nanopores size, wall chemistry, atomic density, and roughness, our EOS is validated to be sufficiently accurate in modeling gas storage behavior in nanoporous materials at supercritical temperature over a wide range of pressure.

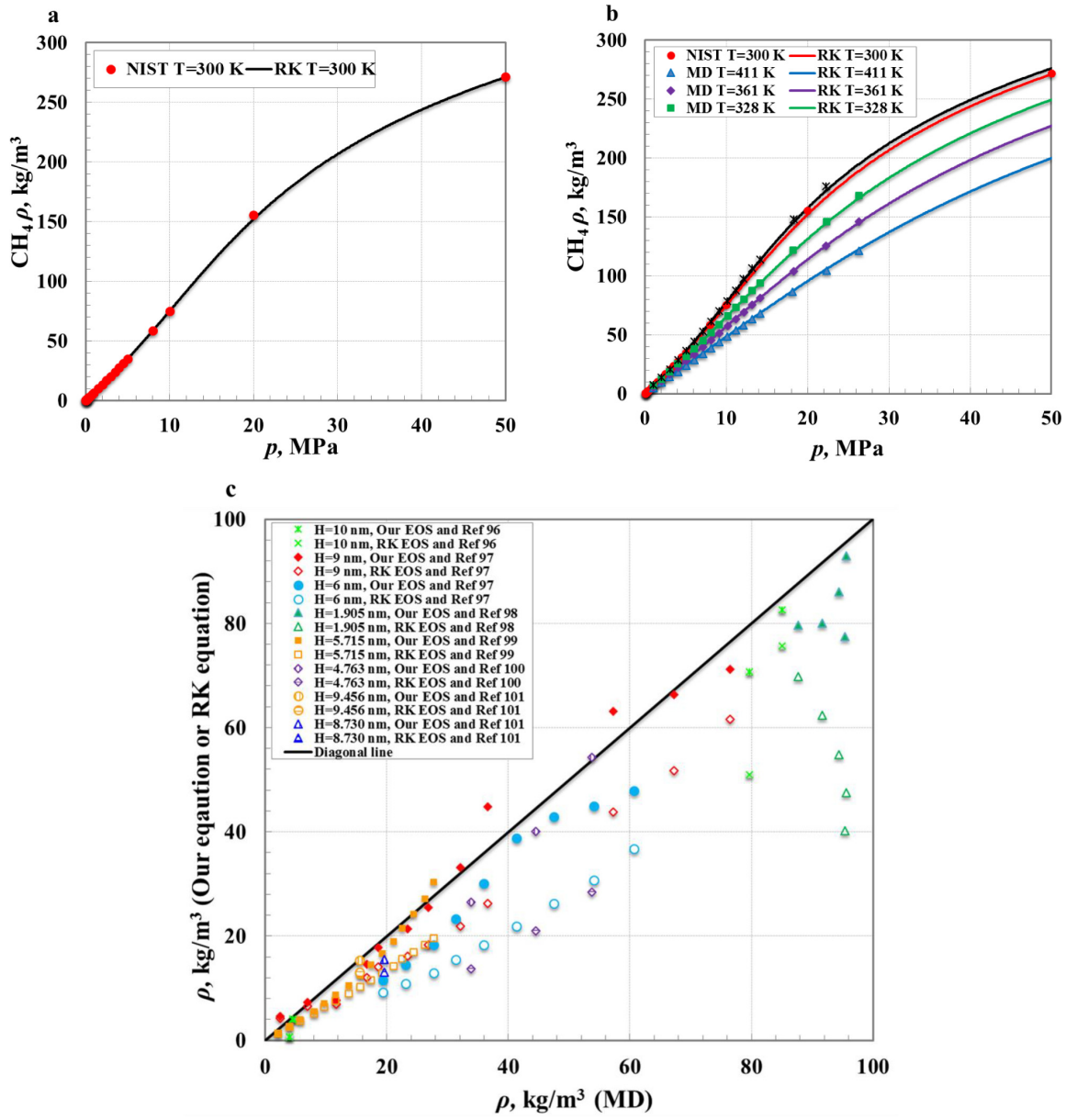

Figure 3—Comparisons of the results calculated by RK EOS and our EOS with data from NIST and MD simulation. (a) Comparison of the results calculated by RK EOS and NIST data; (b) Comparison of the MD simulation data and the results calculated by RK EOS; (c) Comparisons of the results calculated by our EOS and RK EOS, and MD simulation data, respectively. Our EOS improves the prediction accuracy compared with RK EOS. Ref 96: Carbon, slit pore, *T*=298.15K; Ref 97: Graphite, slit pore, *T*=298K; Ref 98: Activated carbon, slit pore, *T*=313.15K; Ref 99: Activated carbon BPL-6, slit pore, *T*=308K; Ref 100: Activated carbon, slit pore, *T*=293K; Ref 101: Activated carbon, slit pore, *T*=308K. Noted that slit pores have been most commonly adopted to model nanopores for investigating gas storage because of their simplicity in MD simulation, while more complex nanopores (cylindrical pores) have been seldom used due to their expensive computation and specialized nature to our knowledge.

Our EOS provides the advantages of simplicity and preciseness due to only one fitted parameter and capturing the key methane storage mechanisms in modeling shale gas storage. In addition, it can quantitatively characterize the relationships between each of property variables with the gas storage behavior in nanoporous material. Thus, we can use it to screen efficiently the existing nanoporous materials, and to sketch the image of the ideal and optimal nanoporous materials for maximizing the gas storage amount.

It is noted that we choose simple pore geometries (cylindrical and slit pores) as nanopore models for deriving the analytical expressions for the varying critical properties and the strength of the gas molecules-wall molecules interaction as elucidated above. In reality, it is impossible to represent a real nanoporous material with the perfect cylindrical or slit pores. We have developed a method to represent a real nanoporous material by an assembly of the cylindrical and slit pores, guaranteeing that the simple pore model has an equivalent nanopore size possessing the same gas storage behavior as the real nanoporous material. We will show that the simple pore model can be applied to reproduce very well the experimental results of gas storage behavior in a real nanoporous material.

Results and discussion

Figure 4 shows that the methane storage amount increases with the increasing pressure in nanopores. However, the methane storage behavior is varying in different pressure regions (see Fig. 4a). In low pressure region, the methane storage amount is larger compared with bulk methane due to the dominance of the interaction between methane molecules and wall that having a positive influence. In high pressure region, it is smaller compared with bulk methane, because that the methane intermolecular interaction dominates, and the interaction between methane molecules and wall becomes a negative influence. In middle pressure regions, it is similar to bulk gas because of the almost equal contributions of both interactions mentioned above. In addition, geometric constraint always has a negative influence on the methane storage amount over all pressure regions. As nanopore size decreases, the interaction between gas molecules and wall gradually becomes strong, the methane storage capacity increases at low pressure, while decreases at high pressure. Moreover, the smaller nanopore has quicker saturation of methane storage due to the overlapping of interactions with opposite walls[11] (see Fig. 4b). Pore shape plays a crucial role in gas storage behavior, with the same pore size, compared with slit pore, the gas storage capacity in cylindrical pore is higher at low pressure, and lower above relatively high pressure, due to the difference of the interactions of methane molecules and wall for both types of pores (see Fig. 4c). In addition, nanopores wall energy sites also control the interaction of methane molecules and wall, and influences the gas storage behavior (see Fig. 4d). The different energy sites on nanopore wall have significant difference in polarizing the methane molecules, and result in difference of the strengths of interaction between methane molecules and wall. These energy sites arise from many sources, such as functional groups (types, number and position), wall atomic density and roughness.

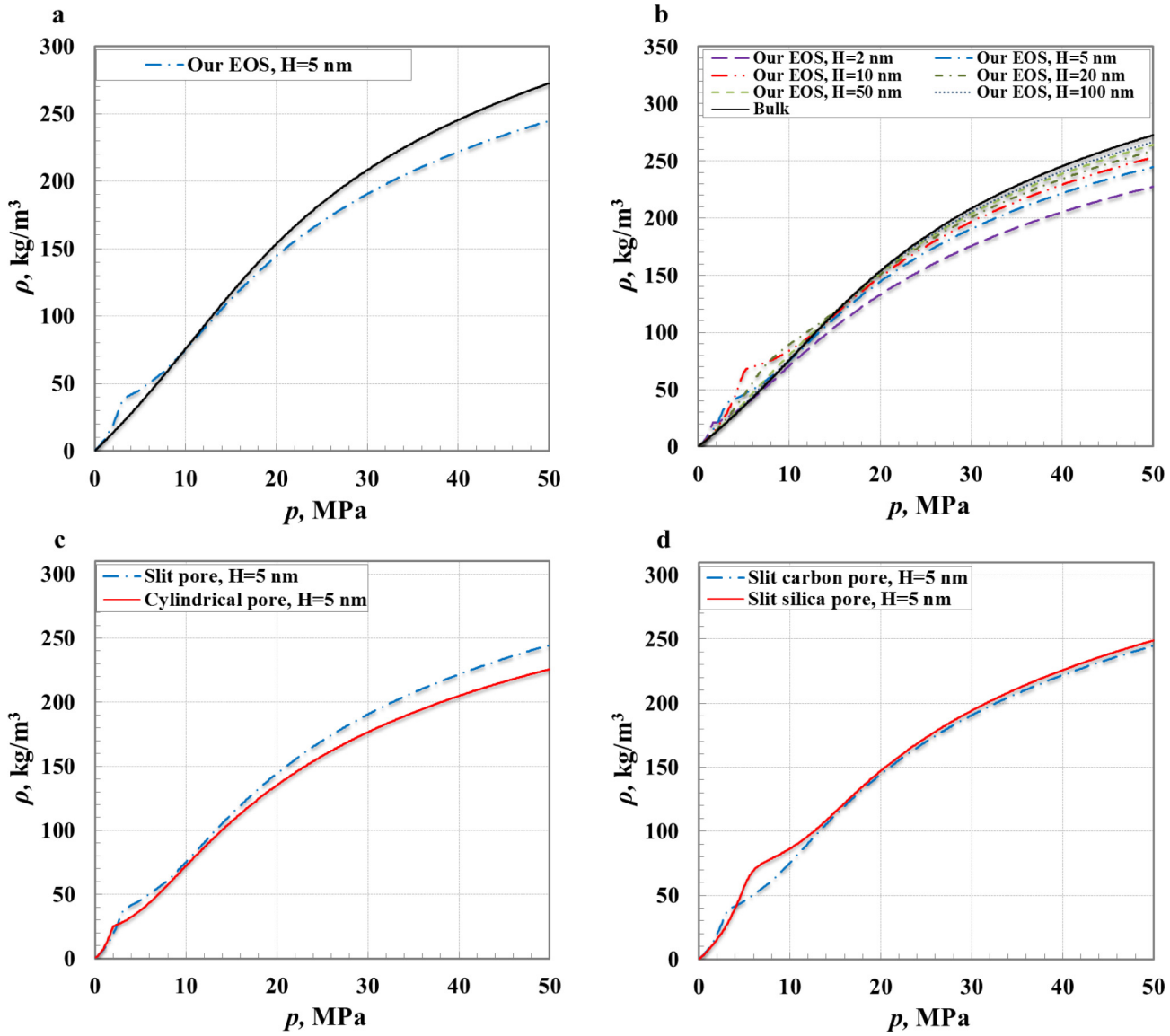

Figure 4—Methane storage behavior in activated carbon pores. (a) Slit activated carbon pores with H=5 nm at T=298.15 K. (b) Slit activated carbon pores with different sizes at T=298.15 K. For comparison, gas storage behavior of bulk gas is represented as a black line. (c) Slit and cylindrical activated carbon pores with H=5 nm at T=298.15 K. (d) Slit activated carbon and silica pores with H=5 nm at T=298.15 K.

Conclusion

In summary, we have developed the EOS for methane in nanoporous materials at supercritical temperature over a wide range of pressure. Our EOS successfully captures the key methane storage mechanisms, and links the methane storage behavior and the microscopic properties including the varying critical properties, the gas intermolecular interaction, and the gas molecules-wall molecules interaction. Our results demonstrate that our EOS is able to relate very well the methane storage behavior with each of key physical parameters, including pore size, shape, wall chemistry and roughness. Moreover, our EOS only requires one fitted parameter, and is simply and powerful in modeling the methane storage in nanoporous shale, and screening the existing nanoporous materials and sketching the image of the optimal candidates of nanoporous materials for methane storage in vehicular application. Also, our EOS can be readily extended to other common gas (CO_2, H_2, N_2, Ar and He), and open up new methods for the related fields

of research, including gas separations[102], carbon capture and storage[103], as well as membranes[104] and catalysis[105].

Acknowledgements

The authors would like to acknowledge the NSERC/AIEES/Foundation CMG and AITF Chairs for providing research funding. The first author also acknowledges the National Natural Science Foundation of China (NO. 51490654 and NO. 51374222) to support part of this work.

References

1. Lee, R. The outlook for population growth. *Science* **333,** 569–573 (2011).
2. Chu, S. & Majumdar, A. Opportunities and challenges for a sustainable energy future. *Nature* **488,** 294–303 (2012).
3. International Energy Agency in World Energy Outlook 2011, 546–547 http://www.worldenergyoutlook.org (International Energy Agency, 2011).
4. Casco, M. E., Martínez-Escandell, M., Gadea-Ramos, E., Kaneko, K., Silvestre-Albero, J. & Rodríguez-Reinoso, F. High-Pressure Methane Storage in Porous Materials: Are Carbon Materials in the Pole Position?. *Chem. Mater.* **27,** 959–964 (2015).
5. Chang, G. et al. A microporous metal–organic framework with polarized trifluoromethyl groups for high methane storage. *Chem. Commun*. **51,** 14789–14792 (2015).
6. Brandt, A. R. et al. Methane leaks from North American natural gas systems. *Science* **343,** 733–735 (2014).
7. Li, B. et al. Porous metal–organic frameworks with Lewis basic nitrogen sites for high-capacity methane storage. *Energy Environ. Sci*. **8,** 2504–2511 (2015).
8. Koh, H. S., Rana, M. K., Wong-Foy, A. G. & Siegel, D. J. Predicting methane storage in open-metal-site MOFs. *J. Phys. Chem. C* **119,** 13451–13458 (2015).
9. Yuan, Q., Zhu, X., Lin, K. & Zhao, Y. P. Molecular dynamics simulations of the enhanced recovery of confined methane with carbon dioxide. *Phys. Chem. Chem. Phys*. **17,** 31887–31893 (2015).
10. Service, R. F. Stepping on the gas. *Science* **346,** 538–541 (2014).
11. Wu, H. A., Chen, J. & Liu, H. Molecular dynamics simulations about adsorption and displacement of methane in carbon nanochannels. *J. Phys. Chem. C* **119,** 13652–13657 (2015).
12. Alezi, D. et al. MOF crystal chemistry paving the way to gas storage needs: Aluminum-based soc-MOF for CH_4, O_2, and CO_2 storage. *J. Am. Chem. Soc*. **137,** 13308–13318 (2015).
13. Vidic, R. D., Brantley, S. L., Vandenbossche, J. M., Yoxtheimer, D. & Abad, J. D. Impact of shale gas development on regional water quality. *Science* **340,** 1235009 (2013).
14. Papaioannou, A. & Kausik, R. Methane storage in nanoporous media as observed via high-field NMR relaxometry. *Physical Review Applied* **4,** 024018 (2015).
15. Yang, R., He, S., Yi, J. & Hu, Q. Nano-scale pore structure and fractal dimension of organic-rich Wufeng-Longmaxi shale from Jiaoshiba area, Sichuan Basin: Investigations using FE-SEM, gas adsorption and helium pycnometry. *Mar. Pet. Geol*. **70,** 27–45 (2016).
16. Beckner, M. & Dailly, A. Adsorbed methane storage for vehicular applications. *Appl Energy* **149,** 69–74 (2015).
17. Simon, C. M. et al. The materials genome in action: identifying the performance limits for methane storage. *Energy Environ. Sci*. **8,** 1190–1199 (2015).
18. Mason, J. A. et al. Methane storage in flexible metal–organic frameworks with intrinsic thermal management. *Nature* **527,** 357–361 (2015).
19. Shen, J., Sulkowski, J., Beckner, M. & Dailly, A. Effects of textural and surface characteristics of metal-organic frameworks on the methane adsorption for natural gas vehicular application. *Micropor. Mesopor. Mater*. **212,** 80–90 (2015).
20. See DOE MOVE program at https://arpa-e-foa.energy.gov/.
21. Peng, Y. et al. Simultaneously high gravimetric and volumetric methane uptake characteristics of the metal–organic framework NU-111. *Chem. Commun*. **49,** 2992–2994 (2013).
22. Makal, T. A., Li, J. -R., Lu, W. & Zhou, H. -C. Methane storage in advanced porous materials. *Chem. Soc. Rev*. **41,** 7761–7779 (2012).
23. Deem, M. W., Pophale, R. & Cheeseman, P. A. A database of new zeolite-like materials. *Phys. Chem. Chem. Phys*. **13,** 12407–12412 (2011).

24. Kim, J. et al. New materials for methane capture from dilute and medium-concentration sources. *Nat. Commun*. **4**:1694 doi: 10.1038/ncomms2697 (2013).
25. Ferey, G. Hybrid porous solids: Past, present, future. *Chem. Soc. Rev*. **37,** 024018 (2008).
26. Yaghi, O. M. et al. Recticular synthesis and the design of new materials. *Nature* **423,** 024018 (2003).
27. D'Alessandro, D. M., Smit, B. & Long, J. R. Carbon dioxide capture: Prospects for new materials. *Angew. Chem. Int. Ed*. **49,** 024018 (2010).
28. Banerjee, R. et al. High-throughput synthesis of zeolitic imidazolate frameworks and application to CO2 capture. *Science* **319,** 024018 (2008).
29. Wang, B., Côté, A. P., Furukawa, H., O'Keeffe, M. & Yaghi, O. M. Colossal cages in zeolitic imidazolate frameworks as selective carbon dioxide reservoirs. *Nature* **453,** 207–211 (2008).
30. Adisa, O. O., Cox, B. J. & Hill, J. M. Methane storage in molecular nanostructures. *Nanoscale* **4,** 3295–3307 (2012).
31. Lu, X. et al. Competitive adsorption of a binary CO_2–CH_4 mixture in nanoporous carbons: effects of edge-functionalization. *Nanoscale* **7,** 1002–1012 (2015).
32. Dawson, R., Cooper, A. I. & Adams, D. J. Nanoporous organic polymer networks. *Prog. Polym. Sci*. **37,** 530–563 (2012).
33. Feng, X., Ding, X. & Jiang, D. Covalent organic frameworks. *Chem. Soc. Rev*. **41,** 6010–6022 (2012).
34. He, Y., Zhou, W., Qian, G. & Chen, B. Methane storage in metal–organic frameworks. *Chem. Soc. Rev*. **43,** 5657–5678 (2014).
35. Peng, Y. et al. Methane storage in metal–organic frameworks: current records, surprise findings, and challenges. *J. Am. Chem. Soc*. **135,** 11887–11894 (2013).
36. Mason, J. A., Veenstra, M. & Long, J. R. Evaluating metal–organic frameworks for natural gas storage. *Chem. Sci*. **5,** 32–51 (2014).
37. Furukawa, H. et al. Ultrahigh porosity in metal-organic frameworks. *Science* **329,** 424–428 (2010).
38. Eddaoudi, M., Sava, D. F., Eubank, J. F., Adil, K. & Guillerm, V. Zeolite-like metal–organic frameworks (ZMOFs): design, synthesis, and properties. *Chem. Soc. Rev*. **44,** 228–249 (2015).
39. Stadie, N. P., Murialdo, M., Ahn, C. C. & Fultz, B. Unusual entropy of adsorbed methane on Zeolite-templated carbon. *J. Phys. Chem. C* **119,** 26409–26421 (2015).
40. Shekhah, O. et al. Made-to-order metal-organic frameworks for trace carbon dioxide removal and air capture. *Nat. Commun*. **5**:4228 doi: 10.1038/ncomms5228 (2014).
41. Nguyen, T. X., Bae, J. S., Wang, Y. & Bhatia, S. K. On the strength of the hydrogen− carbon interaction as deduced from physisorption. *Langmuir* **25,** 4314–4319 (2009).
42. Bartuś, K. & Broódka, A. Temperature study of structure and dynamics of methane in carbon nanotubes. *J. Phys. Chem. C* **118,** 12010–12016 (2014).
43. Eddaoudi, M. et al. Systematic design of pore size and functionality in isoreticular MOFs and their application in methane storage. *Science* **295,** 469–472 (2002).
44. Gadipelli, S. & Guo, Z. X. Graphene-based materials: Synthesis and gas sorption, storage and separation. *Prog. Mater. Sci*. **69,** 1–60 (2015).
45. Wilmer, C. E. et al. Large-scale screening of hypothetical metal–organic frameworks. *Nat. Chem*. **4,** 83–89 (2012).
46. Lasich, M. & Ramjugernath, D. Influence of unlike dispersive interactions on methane adsorption in graphite: a grand canonical Monte Carlo simulation and classical density functional theory study. *Eur. Phys. J. B* **88,** 1–10 (2015).
47. Zhang, H., Deria, P., Farha, O. K., Hupp, J. T. & Snurr, R. Q. A thermodynamic tank model for studying the effect of higher hydrocarbons on natural gas storage in metal–organic frameworks. *Energy Environ. Sci*. **8,** 1501–1510 (2015).
48. Talapatra, S., Zambano, A. Z., Weber, S. E. & Migone, A. D. Gases do not adsorb on the interstitial channels of closed-ended single-walled carbon nanotube bundles. *Phys. Rev. Lett*. **85,** 024018 (2000).
49. Rowsell, J. L., Spencer, E. C., Eckert, J., Howard, J. A. & Yaghi, O. M. Gas adsorption sites in a large-pore metal-organic framework. *Science* **309,** 1350–1354 (2005).
50. Cho, H. S. et al. Extra adsorption and adsorbate superlattice formation in metal-organic frameworks. *Nature* **527,** 503–507 (2015).
51. Drummond, M. L., Sumpter, B. G., Shelton, W. A. & Larese, J. Z. Density functional investigation of the adsorption of a methane monolayer on an MgO (100) surface. *Phys. Rev. B* **73,** 024018 (2006).
52. Zarragoicoechea, G. J. & Kuz, V. A. van der Waals equation of state for a fluid in a nanopore. *Phys. Rev. E* **65,** 024018 (2002).

53. Zhu, X. & Zhao, Y. P. Atomic mechanisms and equation of state of methane adsorption in carbon nanopores. *J. Phys. Chem. C* **118,** 17737–17744 (2014).
54. Shi, W. & Johnson, J. K. Gas adsorption on heterogeneous single-walled carbon nanotube bundles. *Phys. Rev. Lett*. **91,** 024018 (2003).
55. Öström, H., Ogasawara, H., Näslund, L. Å. Pettersson, L. G. M. & Nilsson, A. Physisorption-induced CH bond elongation in methane. *Phys. Rev. Lett*. **96,** 024018 (2006).
56. Jiang, J., Sandler, S. I. & Smit, B. Capillary phase transitions of n-alkanes in a carbon nanotube. *Nano Lett*. **4,** 241–244 (2004).
57. Dimitrakakis, G. K., Tylianakis, E. & Froudakis, G. E. Pillared graphene: a new 3-D network nanostructure for enhanced hydrogen storage. *Nano Lett*. **8,** 3166–3170 (2008).
58. Ockwig, N. W., Delgado-Friedrichs, O., O'Keeffe, M. & Yaghi, O. M. Reticular chemistry: occurrence and taxonomy of nets and grammar for the design of frameworks. *Acc. Chem. Res*. **38,** 176–182 (2005).
59. Lépinay, M. et al. Predicting Adsorption on Bare and Modified Silica Surfaces. *J. Phys. Chem. C* **119,** 6009–6017 (2015).
60. Madani, S. H., Sedghi, S., Biggs, M. J. & Pendleton, P. Analysis of adsorbate–adsorbate and adsorbate–adsorbent interactions to decode isosteric heats of gas adsorption. *ChemPhysChem* **16,** 3797–3805 (2015).
61. García, E. J., Pérez-Pellitero, J., Jallut, C. & Pirngruber, G. D. Modeling Adsorption Properties on the Basis of Microscopic, Molecular, and Structural Descriptors for Nonpolar Adsorbents. *Langmuir* **29,** 9398–9409 (2013).
62. Berland, K. et al. van der Waals forces in density functional theory: a review of the vdW-DF method. *Rep. Prog. Phys*. **78,** 024018 (2015).
63. Lin, L. C. et al. In silico screening of carbon-capture materials. *Nature Mater*. **11,** 633–641 (2012).
64. Petropoulos, J. H. & Papadokostaki, K. G. May the Knudsen equation be legitimately, or at least usefully, applied to dilute adsorbable gas flow in mesoporous media?. *Chem. Eng. Sci*. **68,** 392–400 (2012).
65. Shindo, Y., Hakuta, T., Yoshitome, H. & Inoue, H. (1983). Gas diffusion in microporous media in Knudsen''s regime. *J. Chem. Eng. Jpn.* **16,** 120–126.
66. Koga, K., Gao, G. T., Tanaka, H. & Zeng, X. C. Formation of ordered ice nanotubes inside carbon nanotubes. *Nature* **412,** 802–805 (2001).
67. Holt, J. K. et al. Fast mass transport through sub-2-nanometer carbon nanotubes. *Science* **312,** 1034–1037 (2006).
68. Giovambattista, N., Rossky, P. J. & Debenedetti, P. G. Phase transitions induced by nanoconfinement in liquid water. *Phys. Rev. Lett*. **102,** 024018 (2009).
69. Köfinger, J., Hummer, G. & Dellago, C. Macroscopically ordered water in nanopores. *Proc. Natl Acad. Sci. USA* **105,** 13218–13222 (2008).
70. Gelb, L. D., Gubbins, K. E., Radhakrishnan, R. & Sliwinska-Bartkowiak, M. Phase separation in confined systems. *Rep. Prog. Phys*. **62,** 1573–1659 (1999).
71. Alba-Simionesco, C. et al. Effects of confinement on freezing and melting. *J. Phys.: Condens. Matter* **18,** R15–R68 (2006).
72. Porcheron, F., Monson, P. A. & Thommes, M. Modeling mercury porosimetry using statistical mechanics. *Langmuir* **20,** 6482–6489 (2004).
73. Pellenq, R. J. M. Coasne, B., Denoyel, R. O. & Coussy, O. Simple phenomenological model for phase transitions in confined geometry. 2. Capillary condensation/evaporation in cylindrical mesopores. *Langmuir* **25,** 1393–1402 (2009).
74. Noy, A. et al. Nanofluidics in carbon nanotubes. *Nano Today* **2,** 22–29 (2007).
75. Zhang, X. & Wang, W. Square-well fluids in confined space with discretely attractive wall-fluid potentials: Critical point shift. *Phys. Rev. E* **74,** 024018 (2006).
76. Derycke, I., Vigneron, J. P., Lambin, P., Lucas, A. A. & Derouane, E. G. Physisorption in confined geometry. *J. Chem. Phys*. **94,** 4620–4627 (1991).
77. Hamada, Y., Koga, K. & Tanaka, H. Phase equilibria and interfacial tension of fluids confined in narrow pores. *J. Chem. Phys*. **127,** 024018 (2007).
78. Singh, S. K. & Singh, J. K. Effect of pore morphology on vapor–liquid phase transition and crossover behavior of critical properties from 3D to 2D. *J. Fluid Phase Equilib*. **300,** 182–187 (2011).
79. Islam, A. W., Patzek, T. W. & Sun, A. Y. Thermodynamics phase changes of nanopore fluids. *J. Nat. Gas Sci. Eng*. **25,** 134–139 (2015).
80. Zarragoicoechea, G. J. & Kuz, V. A. Critical shift of a confined fluid in a nanopore. *J. Fluid Phase Equilib*. **220,** 7–9 (2004).

81. Morishige, K., Fujii, H., Uga, M. & Kinukawa, D. Capillary critical point of argon, nitrogen, oxygen, ethylene, and carbon dioxide in MCM-41. *Langmuir* **13,** 3494–3498 (1997).
82. Pitakbunkate, T., Balbuena, P., Moridis, G. J. & Blasingame, T. A. Effect of confinement on PVT properties of hydrocarbons in shale reservoirs. In SPE Annual Technical Conference and Exhibition. Society of Petroleum Engineers, (2014).
83. Didar, B. R. & Akkutlu, I. Y. Pore-size dependence of fluid phase behavior and properties in organic-rich shale reservoirs. In SPE international symposium on oilfield chemistry. Society of Petroleum Engineers, (2013).
84. Singh, S. K., Saha, A. K. & Singh, J. K. Molecular Simulation Study of Vapor− Liquid Critical Properties of a Simple Fluid in Attractive Slit Pores: Crossover from 3D to 2D. *J. Phys. Chem. B* **114,** 4283–4292 (2010).
85. Singh, S. K., Sinha, A., Deo, G. & Singh, J. K. Vapor− liquid phase coexistence, critical properties, and surface tension of confined alkanes. *J. Phys. Chem. C* **113,** 7170–7180 (2009).
86. Vishnyakov, A., Piotrovskaya, E. M., Brodskaya, E. N., Votyakov, E. V. & Tovbin, Y. K. Critical properties of Lennard-Jones fluids in narrow slit-shaped pores. *Langmuir* **17,** 4451–4458 (2001).
87. Jana, S., Singh, J. K. & Kwak, S. K. Vapor-liquid critical and interfacial properties of square-well fluids in slit pores. *J. Chem. Phys*. **130,** 024018 (2009).
88. Bhatia, S. K., Bonilla, M. R. & Nicholson, D. Molecular transport in nanopores: a theoretical perspective. *Phys. Chem. Chem. Phys*. **13,** 15350–15383 (2011).
89. Tjatjopoulos, G. J., Feke, D. L. & Mann Jr, J. A. Molecule-micropore interaction potentials. *J. Phys. Chem*. **92,** 4006–4007 (1988).
90. Steele, W. A. The physical interaction of gases with crystalline solids: I. Gas-solid energies and properties of isolated adsorbed atoms. *Surf. Sci*. **36,** 317–352 (1973).
91. Balbuena, P. B. & Gubbins, K. E. Theoretical interpretation of adsorption behavior of simple fluids in slit pores. *Langmuir* **9,** 1801–1814 (1993).
92. Redlich, O. & Kwong, J. N. On the thermodynamics of solutions. V. An equation of state. Fugacities of gaseous solutions. *Chem. Rev*. **44,** 233–244 (1949).
93. Whitson, C. H. & Brulé, M. R. Phase behavior. Henry L. Doherty Memorial Fund of AIME, Society of Petroleum Engineers, (2000).
94. Setzmann, U. & Wagner, W. A new equation of state and tables of thermodynamic properties for methane covering the range from the melting line to 625 K at pressures up to 100 MPa. *J. Phys. Chem. Ref. Data* **20,** 1061–1155 (1991).
95. Kowalczyk, P., Tanaka, H., Kaneko, K., Terzyk, A. P. & Do, D. D. Grand canonical Monte Carlo simulation study of methane adsorption at an open graphite surface and in slitlike carbon pores at 273 K. *Langmuir* **21,** 5639–5646 (2005).
96. Jin, Z. & Firoozabadi, A. Flow of methane in shale nanopores at low and high pressure by molecular dynamics simulations. *J. Chem. Phys*. **143,** 024018 (2015).
97. Mosher, K., He, J., Liu, Y., Rupp, E. & Wilcox, J. Molecular simulation of methane adsorption in micro-and mesoporous carbons with applications to coal and gas shale systems. *Int. J. Coal Geol*. **109,** 36–44 (2013).
98. Jiang, S., Zollweg, J. A. & Gubbins, K. E. High-pressure adsorption of methane and ethane in activated carbon and carbon fibers. *J. Phys. Chem*. **98,** 5709–5713 (1994).
99. Gusev, V. Y., O'Brien, J. A. & Seaton, N. A. A self-consistent method for characterization of activated carbons using supercritical adsorption and grand canonical Monte Carlo simulations. *Langmuir* **13,** 2815–2821 (1997).
100. Heuchel, M., Davies, G. M., Buss, E. & Seaton, N. A. Adsorption of carbon dioxide and methane and their mixtures on an activated carbon: simulation and experiment. *Langmuir* **15,** 8695–8705 (1999).
101. Davies, G. M., Seaton, N. A. & Vassiliadis, V. S. Calculation of pore size distributions of activated carbons from adsorption isotherms. *Langmuir* **15,** 8235–8245 (1999).
102. Li, J. R., Sculley, J. & Zhou, H. C. Metal–organic frameworks for separations. *Chem. Rev*. **112,** 869–932 (2012).
103. Sumida, K. et al. Carbon dioxide capture in metal–organic frameworks. *Chem. Rev*. **112,** 724–781 (2011).
104. Dai, Y., Johnson, J. R., Karvan, O., Sholl, D. S. & Koros, W. J. Ultem®/ZIF-8 mixed matrix hollow fiber membranes for CO 2/N 2 separations. *J. Membr. Sci*. **401,** 76–82 (2012).
105. Lee, J. et al. Metal–organic framework materials as catalysts. *Chem. Soc. Rev*. **38,** 1450–1459 (2009).